European Journal of Medicinal Chemistry 313 (2026) 118906

Contents lists available at ScienceDirect

European Journal of Medicinal Chemistry

journal homepage: www.elsevier.com/locate/ejmech

Large-scale structure-based virtual screening identifies diverse $K_{Na}1.1$ (KCNT1) potassium channel inhibitors

Emily A. Caseley [a], Katie J. Simmons [a,b], Bethan A. Cole [a,1], Alex J. Flynn [a,b,2], Stephen P. Muench [a,b], Jonathan D. Lippiat [a,*]

[a] School of Biomedical Sciences, University of Leeds, Leeds, LS2 9JT, UK
[b] Astbury Centre for Structural and Molecular Biology, University of Leeds, Leeds, LS2 9JT, UK

ARTICLE INFO

Keywords:
Potassium channel
$K_{Na}1.1$
KCNT1 epilepsy
Virtual screening
thallium flux
Patch clamp electrophysiology
Molecular docking

ABSTRACT

Severe drug-resistant childhood epilepsy is caused by *KCNT1* gain-of-function genetic variants, resulting in increased $K_{Na}1.1$ channel activity. *KCNT1*-associated epilepsy is thought to affect around 1 in 300,000 births worldwide. Current treatment for KCNT1 epilepsy only provides mild symptomatic relief and uses a cocktail of experimental medications which must be personalised for the individual and are often poorly tolerated. Critically, with many patients, no therapeutic benefit is achieved. We sought to address this by using large-scale virtual screening to accelerate the development of a molecule which binds directly to KCNT1 to supress overactivity. We purchased a total of 71 compounds and using a combination of fluorescent thallium flux assays and patch clamp electrophysiology, identified a series of eight structurally diverse, novel inhibitors of the $K_{Na}1.1$ channel with potency in the low micromolar range. These provide potential starting points for further development of drugs to treat *KCNT1*-associated epilepsy.

1. Introduction

Potassium (K^+) ion channels are among the most widely distributed group of ion channels and comprise a superfamily of structurally and functionally diverse proteins. Within this group, the SLO subfamily of four K^+ channels are among the most complex and exhibit unusually high conductance [1]. The *KCNT1* gene lies within this family and encodes the largest known potassium channel subunit, $K_{Na}1.1$ (also known as SLACK, Slo2.2 or $K_{Ca}4.1$) [2]. This subunit is composed of six transmembrane alpha helices, with a selectivity filter formed by a loop between the fifth and sixth helices, and two intracellular C-terminal regulation of conductance of potassium (RCK) domains [3,4]. This subunit forms a homotetrameric sodium (Na^+)-activated K^+ channel, but can also form heteromeric coassemblies with the closely related $K_{Na}1.2$ subunit (encoded by *KCNT2*) where they colocalise in distinct regions of the central nervous system (CNS) [5,6]. $K_{Na}1.1$-containing channels are activated by millimolar concentrations of sodium (Na^+) and contribute to Na^+-dependent K^+ currents (I_{KNa}). These channels play a role in generating the slow afterhyperpolarisation (AHP) following single [7,8] or bursts of action potential firing [9], in addition to contributing to the resting membrane potential and intrinsic excitability of different cell types in the CNS [10,11] and vascular smooth muscle [12].

Pathogenic gain-of-function (GoF) variants of the *KCNT1* gene are associated with rare and severe forms of drug-resistant epilepsy [13]. More than 50 reported missense variants have been implicated in a range of disorders, most commonly epilepsy of infancy with migrating focal seizures (EIMFS) [14] or autosomal dominant sleep-related hypermotor epilepsy (ADSHE) [15], with less common and more recently discovered phenotypes such as Ohtahara syndrome [16], West syndrome [17], and Lennox-Gastaut syndrome [18]. These conditions are often debilitating; patients present with recurrent seizures, with associated comorbidities including developmental delay or regression and intellectual disabilities [19,20].

The refractoriness to conventional antiepileptic medications seen in these conditions has led to trials with alternative medications such as

This article is part of a special issue entitled: Comp small drug design published in European Journal of Medicinal Chemistry.

* Corresponding author.
E-mail address: j.d.lippiat@leeds.ac.uk (J.D. Lippiat).
[1] Present address: Department of Biochemical and Cellular Pharmacology, Genentech, 103 DNA Way, South San Francisco, CA 94080, USA.
[2] Present address: Simons Electron Microscopy Center, New York Structural Biology Center, New York, NY 10027, USA.

https://doi.org/10.1016/j.ejmech.2026.118906
Received 16 October 2025; Received in revised form 10 April 2026; Accepted 24 April 2026
Available online 25 April 2026

quinidine, a class I antiarrhythmic agent which inhibits $K_{Na}1.1$ channels [21]. However, despite moderate improvements being observed in a small subset of patients, this treatment is largely ineffective [22–24] and can lead to severe cardiotoxicity due to quinidine's lack of specificity and its high degree of potency at cardiac ion channels such as $K_V11.1$ (hERG) [25]. Recently, a patient with the GoF *KCNT1* S937G mutation showed a drastic reduction in seizure activity following treatment with the antidepressant drug fluoxetine, which is also a $K_{Na}1.1$ channel inhibitor [26]. However, whether this is a viable treatment strategy for the majority of patients within this heterogenous group of epilepsy phenotypes is yet to be seen from this n = 1 study; as such, the discovery of further $K_{Na}1.1$ channel inhibitors have potential for both the development of therapies and as tool compounds to interrogate functional properties of this channel in future studies.

To this end, efforts towards discovering small molecules for the specific pharmacological modulation of $K_{Na}1.1$ potassium ion channels have seen an increase in recent years (Fig. 1) [27–31]. Similarly, there have been recent advancements in the availability of high-resolution structural information available from cryo-electron microscopy (cryo--EM) structures of the $K_{Na}1.1$ channel in different conformations [3,4, 32]. We have previously shown that known $K_{Na}1.1$ channel inhibitors typically bind to the inner pore vestibule [27], and the combination of this structural and functional understanding of the channel facilitates the use of a computer-aided approach for the discovery of novel channel modulators. Such as approach can drastically reduce the time and cost of drug development by precluding the requirement for the functional screening of large compound libraries [33].

We aimed to build on our previous structure-based approach by significantly increasing the magnitude of the screen, using high-performance computing, from 10^5 compounds [27] to over 10^6 against the same target. We envisaged that this would increase the chemical diversity of our pool of inhibitors. In this study, we used a virtual high-throughput approach to screen a diverse library of commercially available compounds against the pore of the $K_{Na}1.1$ cryo-electron microscopy structure [3]. Using a combination of fluorescent thallium flux assays and patch clamp electrophysiology, we identified a series of eight structurally diverse, novel inhibitors of the $K_{Na}1.1$ channel with potency in the low micromolar range. Interestingly, new structural information which emerged following the discovery of these inhibitors [4] provided a further insight into the potential binding modes of these compounds, developing our capacity to expand our approach in future studies.

2. Results and discussion

2.1. Structure-based virtual screening

In our previous work, we used a structure-based approach to identify the binding site of the known $K_{Na}1.1$ potassium ion channel inhibitors, bepridil and quinidine, in the intracellular pore vestibule, proximal to the selectivity filter (Fig. 2A). Informed by this, we virtually screened a library of 100,000 drug-like molecules against this site, and of the 17 compounds tested *in vitro*, six were identified as $K_{Na}1.1$ inhibitors [27]. In the present study, we sought to determine whether we could scale this structure-based methodology to screen millions of compounds using high-throughput and high-performance computational tools. We performed virtual screening of different compound libraries against the same site in the chicken $K_{Na}1.1$ cryo-electron microscopy structure in the putative active conformation (PDB 5U70), encompassing side chains from the selectivity filter and S6 transmembrane region which comprise the intracellular pore vestibule (Fig. 2A). The amino acids contained in this region are highly conserved between the chicken and human proteins, with 96% sequence identity (Fig. 2B). For this study we focused our efforts on commercially available libraries of compounds, beginning with our in-house library (MCCB) of approximately 25,000 compounds at the University of Leeds, in addition to the Enamine drug-like and Otava screening collection libraries, containing approximately 1.8 million and 270,000 compounds, respectively. For Enamine, the larger of the three libraries, we adopted a two-fold virtual screening approach wherein the compounds were initially docked using the fast docking

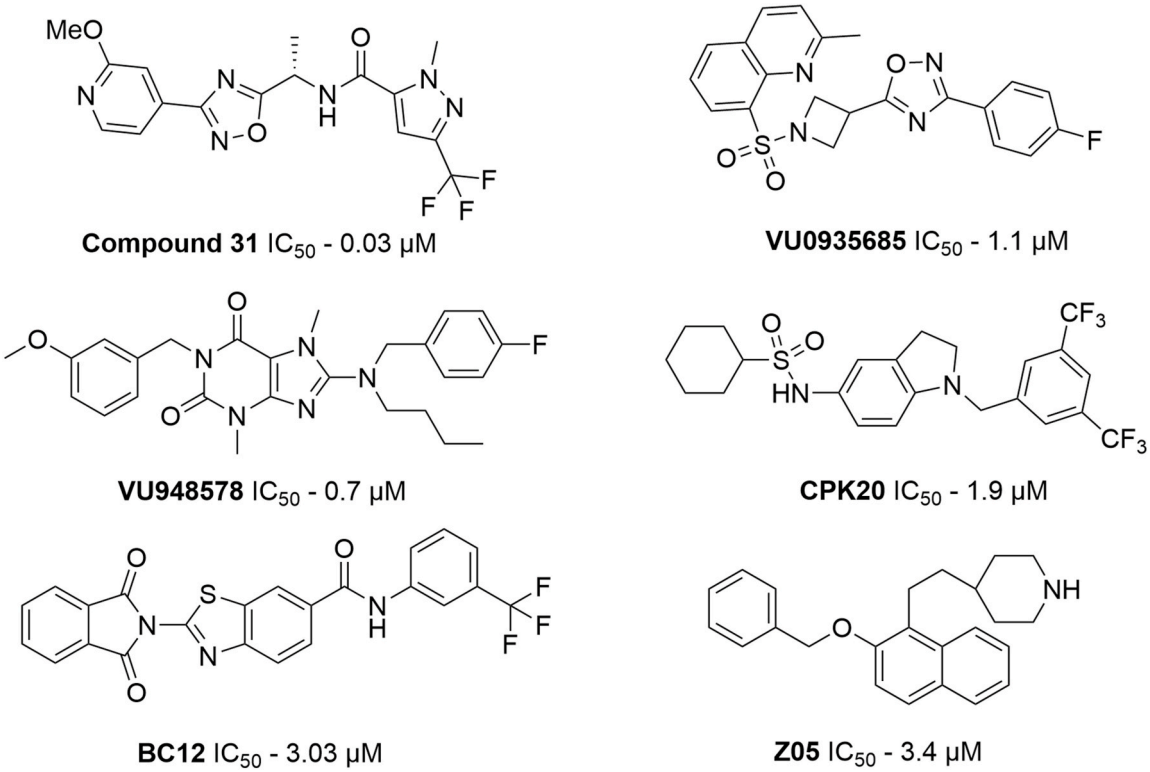

Fig. 1. Structures of representative $K_{Na}1.1$ potassium channel inhibitors and their IC_{50} values against the wild-type human $K_{Na}1.1$ channel.

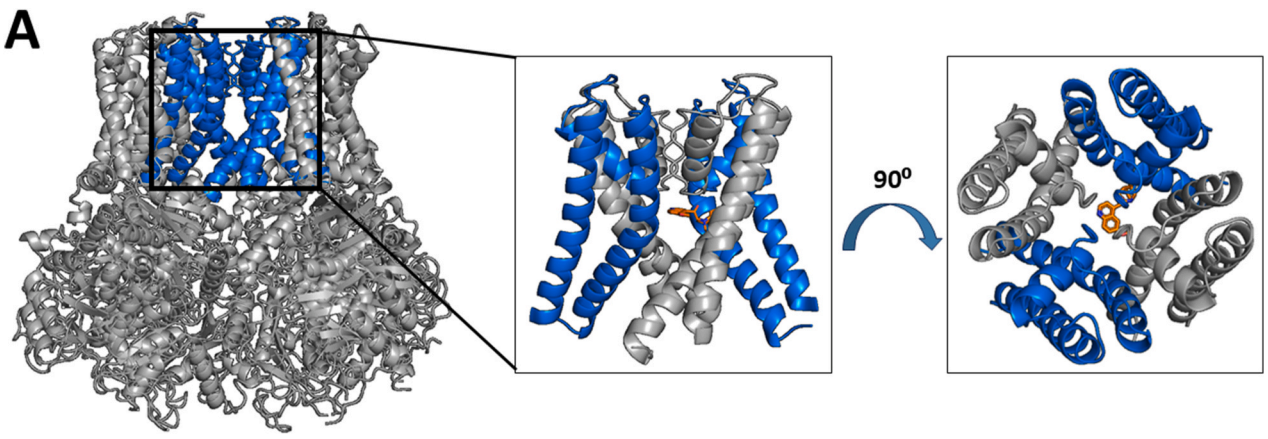

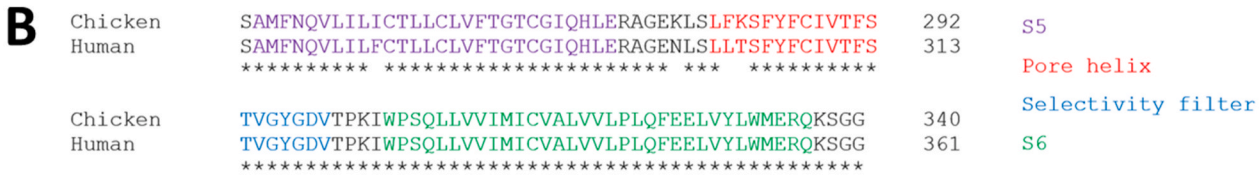

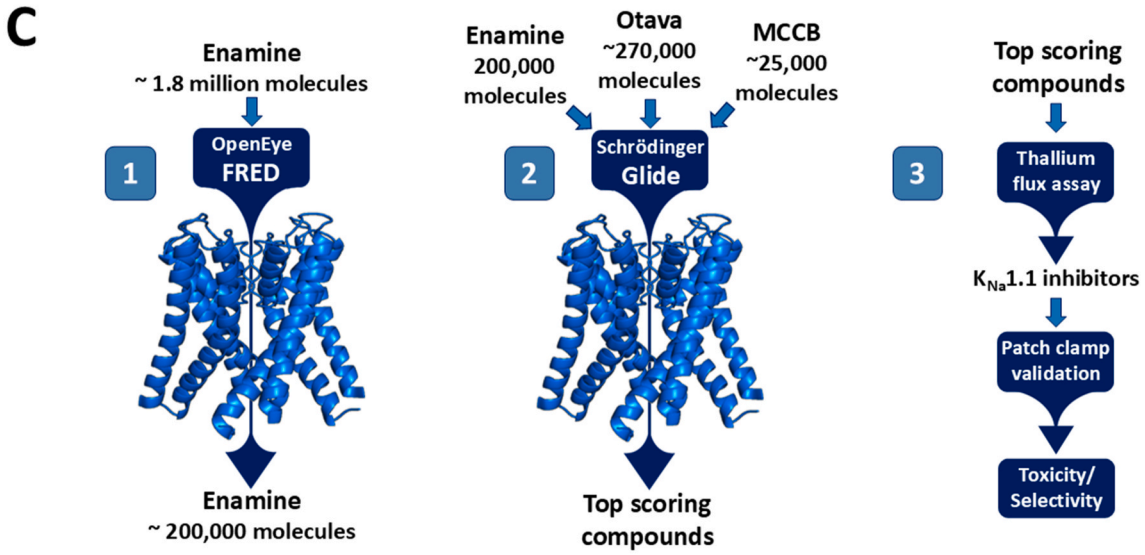

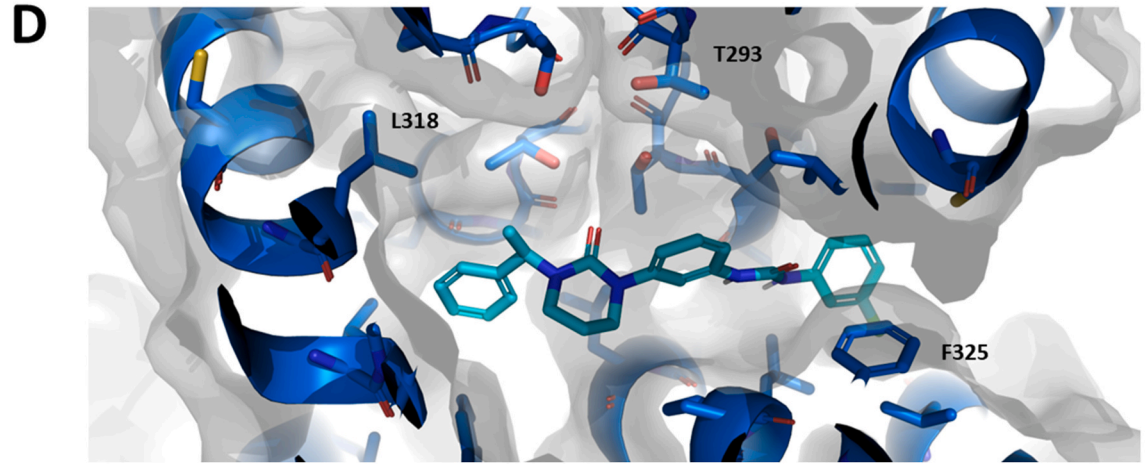

(caption on next page)

Fig. 2. Virtual high throughput screening of chemical libraries to find inhibitors of $K_{Na}1.1$. (A) The tetrameric $K_{Na}1.1$ chicken cryo-EM structure in the open state (PDB 5U70) with the known inhibitor bepridil (orange) docked to a known binding site below the selectivity filter. Inset boxes show the 20 Å cubed region against which screening was carried out, shown parallel to the membrane (left) and from the extracellular side (right). (B) Sequence alignment of the chicken and human $K_{Na}1.1$ channel homologue sequences for the 20 Å cube used in virtual high throughput screens; conserved residues are indicated by an asterisk. (C) Workflow for docking large scale libraries against the $K_{Na}1.1$ structure, including selecting the top 10% predicted highest affinity binding molecules via an initial screen using FRED (OpenEye), then screening this smaller library using Glide (Schrödinger), after which the top scoring commercially available compounds were functionally screened for inhibition comparable to the positive control (100 μM bepridil). (D) Predicted bound conformation of compound **1** in the open chicken $K_{Na}1.1$ potassium ion channel structure (PDB 5U70). Protein shown as blue ribbons with key residues shown as blue sticks and compound 1 shown as cyan sticks.

tool, Fred (Openeye Scientific Software) using high-performance computing, after which the compounds with the top 10 % predicted binding scores from the Enamine library were docked along with the Otava and MCCB libraries using Glide (Schrödinger) in Standard Precision (SP) mode. Compounds from all libraries were ranked by their Glide SP docking score, and those with a docking score greater than −6 discarded. Any pan assay interference compounds (PAINS) [34] were removed, and from the top scoring compounds, 71 were selected based on structural diversity and obtained for further *in vitro* assessment. The workflow for this approach is shown in Fig. 2C.

2.2. *In vitro* validation of selected compounds

To assess whether the compounds selected from the virtual high throughput screen act as $K_{Na}1.1$ potassium ion channel modulators, we initially used a medium-throughput fluorescent thallium flux assay in HEK293 cells stably expressing a heteromer of the wild-type (WT) and GoF mutant Y796H $K_{Na}1.1$ [15]. This heteromeric system was chosen to better represent the response of endogenous channels containing mutant $K_{Na}1.1$ subunits in vivo; *KCNT1*-associated epilepsy patients are generally heterozygous, and channels formed by co-assemblies of the WT and mutant subunits display intermediate properties between homomeric channels [13]. Compounds were initially applied at 10 μM to determine their effects on thallium conductance through $K_{Na}1.1$ channels and compared to cells treated with the known $K_{Na}1.1$ inhibitor, 100 μM bepridil. Cells were loaded with thallium sensitive dye and incubated with or without compounds of interest, following which 2.5 mM Tl_2SO_4 was added after 30 s of background fluorescence readings. Supplementary Fig. 1 illustrates how 5 mM final Tl^+ was selected as ≈ EC_{80} concentration suitable for inhibitor studies and validation of the assay with bepridil (IC_{50} of 9.5 μM obtained). The slope of the resulting fluorescent reads following Tl^+ addition was used to determine which compounds reduced Tl^+ influx to levels comparable to the bepridil control (Fig. 3A). This equated to approximately 50% inhibition due to the presence of endogenous cation ion channels and transporters in HEK293 cells that also conduct thallium ions [35]. From the top compounds virtually screened from the MCCB, Enamine and Otava libraries, 19% showed levels of inhibition at least half that of 100 μM bepridil. The potency of the $K_{Na}1.1$ hits was initially evaluated using a thallium flux assay in cells pre-incubated in varying concentrations of the compound (Fig. 3B and C, and Supplementary Fig. 2A), and eight compounds that had an IC_{50} value < 15 μM using this assay were taken forward for further pharmacological characterisation. Other compounds from the initial 10 μM assay are summarised in Supplementary Table 1. The eight compounds that were selected for further analysis were all confirmed as inhibitors by patch clamp electrophysiology (Fig. 3C and Supplementary Fig. 2B; Table 1). A WST-1 Cell Viability Assay was used to examine compound toxicity in HEK293 cells. With the exception of compound **3**, none affected cell viability at concentrations up to 30 μM (Fig. 4).

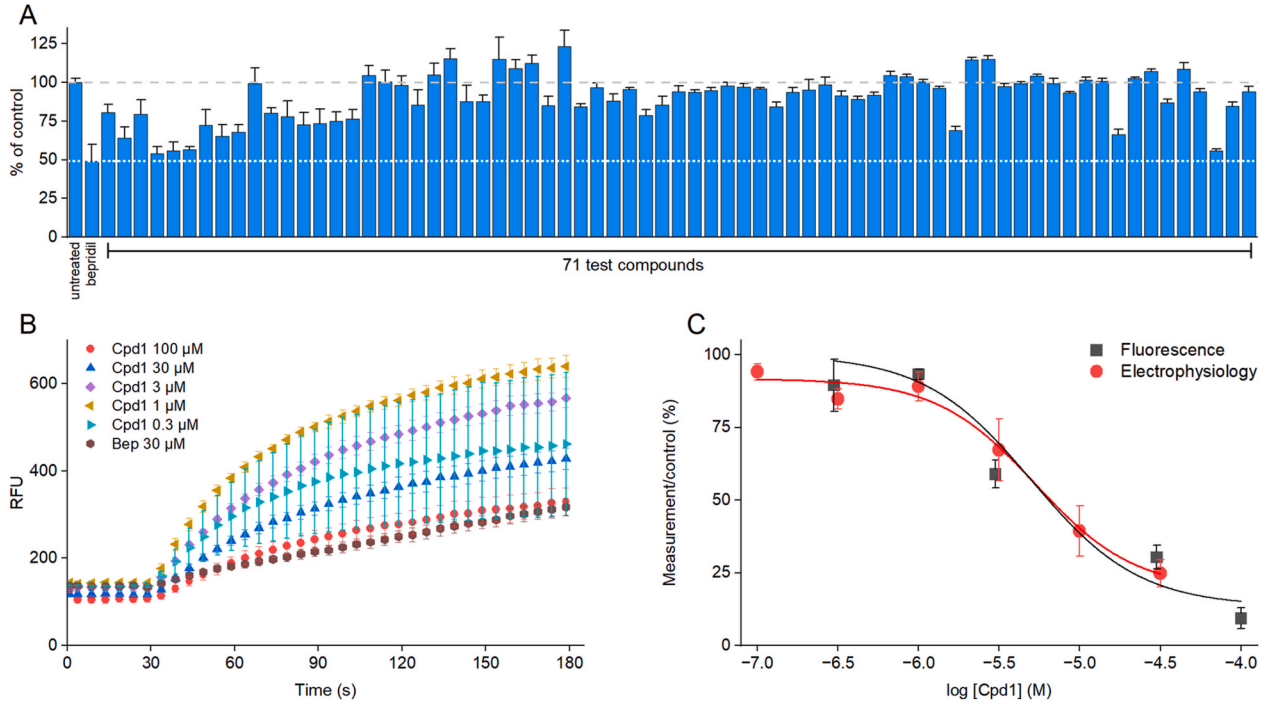

Fig. 3. *In vitro* validation of top scoring compounds identified through virtual high throughput screening. (A) Thallium flux measured from stable HEK293 $K_{Na}1.1$ WT/Y796H cells incubated with test compounds at 10 μM. The grey dashed line indicates the control response in the absence of inhibiter and the white dotted line indicates the inhibition by the positive control, 100 μM bepridil. (B) Representative mean thallium flux data showing thallium-induced fluorescence in response to cell incubation with varying concentrations of compound 1. (C) Concentration-inhibition curves of compound **1** assessed using thallium fluorescence and patch clamp electrophysiology. See Supplementary Fig. 2 for concentration-inhibition data for all 8 compounds.

Table 1
Selected compounds and their potencies (mean IC_{50} values) in inhibiting $K_{Na}1.1$ channels measured using thallium fluorescence and validated by patch clamp electrophysiology.

ID	Structure	IC_{50} (μM)	
		Thallium flux	Patch clamp
1	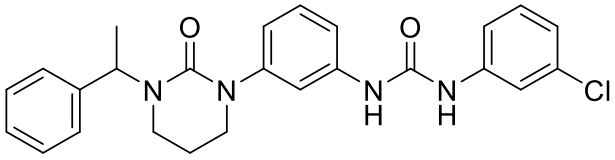	4.7	5.3
2	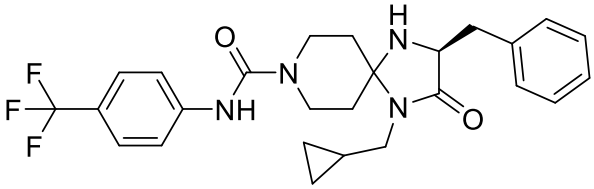	11.9	5.9
3	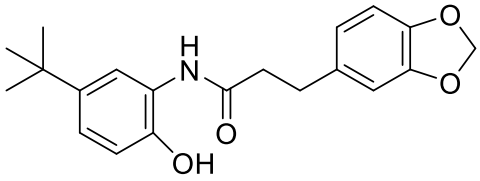	3.1	14.1
4	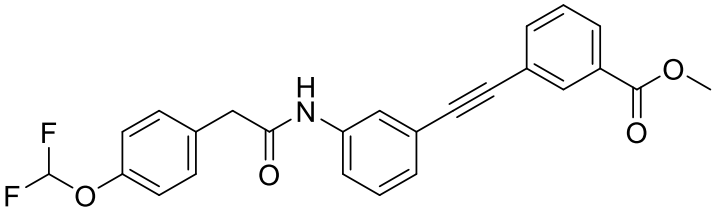	5.9	29.1
5	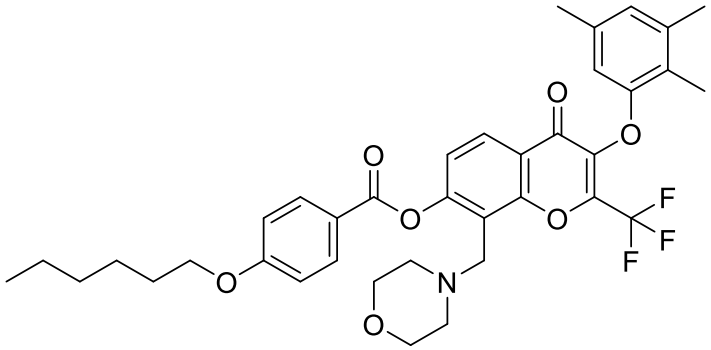	2.6	9.2
6	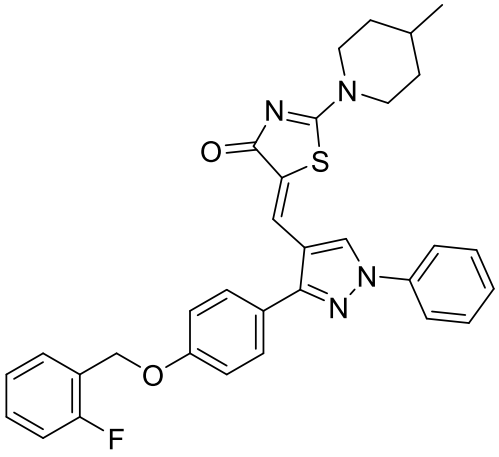	2.4	42.6

(*continued on next page*)

Table 1 (*continued*)

ID	Structure	IC_{50} (μM)	
		Thallium flux	Patch clamp
7	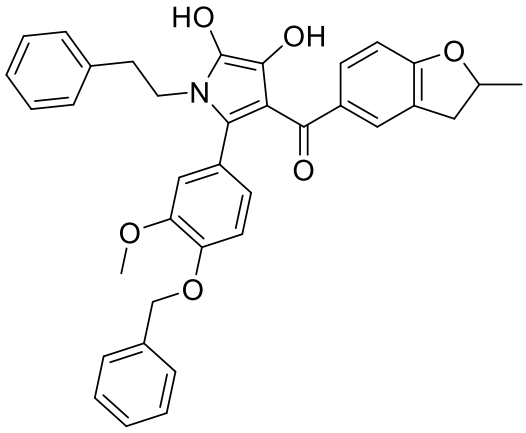	4.9	2.0
8	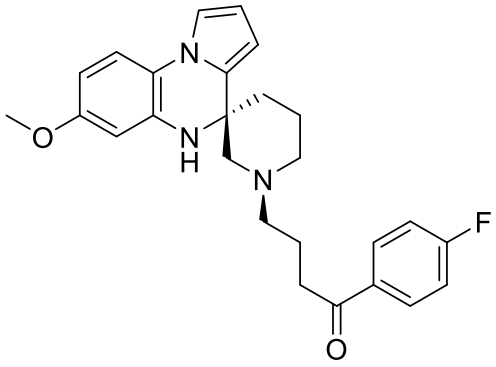	6.7	4.2

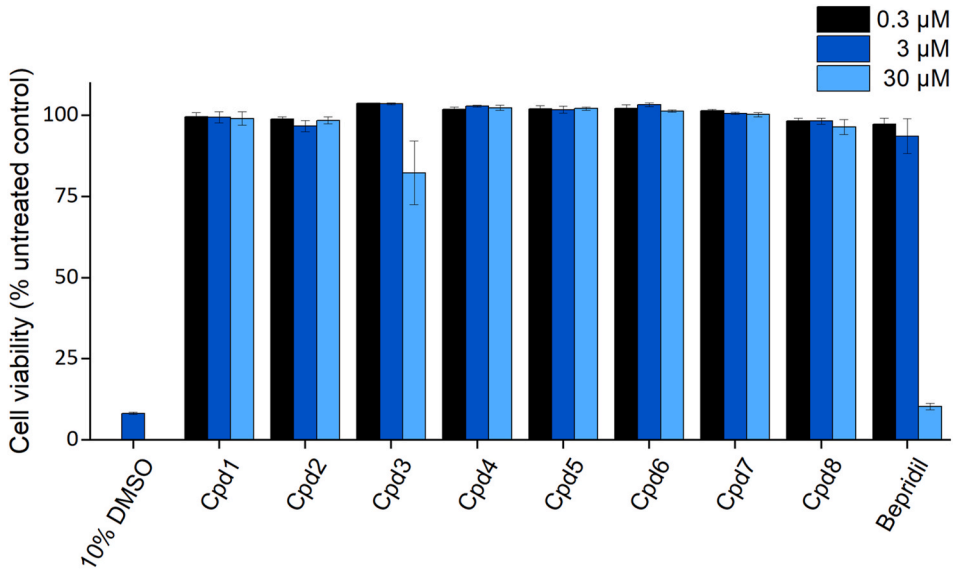

Fig. 4. Summary of percentage of cell viability of HEK293 cells treated for 24 h with the indicated concentration of compound, as determined by WST-1 assay, with 10 % DMSO as a positive control.

2.3. $K_{Na}1.1$ inhibitor selectivity

The selectivity profile of quinidine as a treatment for KCNT1-associated has been a significant barrier to reaching therapeutic doses without significant adverse effects. Further characterization of compounds **1**–**8** included an assessment of potential secondary activity across a panel of seven other potassium channels, including channels encoded by other members of the *Slo* gene family, at 10 μM compound concentration using the thallium flux assay in HEK293 cells stably expressing channels of interest. Most compounds showed a relatively clean selectivity profile, with only compounds **1** and **3** showing greater than 20% channel inhibition for $K_V4.2$. Blockade of hERG potassium

channels is a major cause for pro-arrhythmic effects associated with QT prolongation and torsade-des-pointes in humans. Using patch clamp, it was determined that a number of these compounds (**2**,**3** and **6**) inhibit the hERG channel by over 50% at 10 μM (Fig. 5). Conversely, several of these compounds, for example compound **7** and **8** exhibit very little inhibition of the channel, demonstrating the value of the *in-silico* approach to identify diverse novel channel modulators.

2.4. Predicted binding mode in $K_{Na}1.1$ channel structures

The virtual high throughput screening was carried out using the cryo-EM structure of the pore region of the chicken $K_{Na}1.1$ channel [3] as an expansion of our previous research [27]. We had previously validated the domain targetted by the docking through mutagenesis of F346 that was predicted to contribute to binding of both quinidine and bepridil. F346 is in the sixth transmembrane domain and faces into the intracellular pore vestibule and mutations reduced inhibition by the known and the novel inhibitors reported. The chicken and human proteins are highly homologous, with 96% sequence identity within the region targeted in our virtual high throughput screening (Fig. 2A). The sequence of the inner pore vestibule is conserved between species (Fig. 2B), meaning that the chicken $K_{Na}1.1$ structures are likely to be a reliable model for the interaction of inhibitors with the human $K_{Na}1.1$ channels. More recently, cryo-EM structures of the human $K_{Na}1.1$ channel have been published [4]. This series of structures showed the human $K_{Na}1.1$ ion channel in open, closed and inhibitor-bound states, at resolutions ranging between 2.6 and 3.2 Å. The inhibitor-bound structure elucidated for the first time, the binding mode of a potent $K_{Na}1.1$ channel inhibitor [29] in the intracellular pore domain. The ligand-bound human structure showed movement of the Phe312 side chain into a previously unseen position, exposing a binding pocket that could accommodate part of the inhibitor between the pore helix and the proximal region of the S6 helix. Future *in silico* studies can utilise these structures to further improve the screening cascade for inhibitor identification. Supplementary Fig. 3 shows the top-scoring pose of compounds **1**–**8** with chicken $K_{Na}1.1$ in the open and inhibitor-bound human $K_{Na}1.1$ conformations. Best docking scores for each of compounds **1**–**8** with a range of published $K_{Na}1.1$ structures are summarised in Supplementary Table 2. Whilst most compounds show comparable (or even improved) predicted binding affinities to the recently published inhibitor bound human structure compared to the chicken open state-there are some, e.g. compounds **2** and **5**, for which a loss of affinity to this state is predicted. Therefore, we can suggest that not all compounds that bind to the pore region of the channel invoke the conformational change seen by residue Phe312. Future work using molecular dynamics simulations could begin to elucidate the conformational changes of the channel that occur upon binding this series of inhibitors.

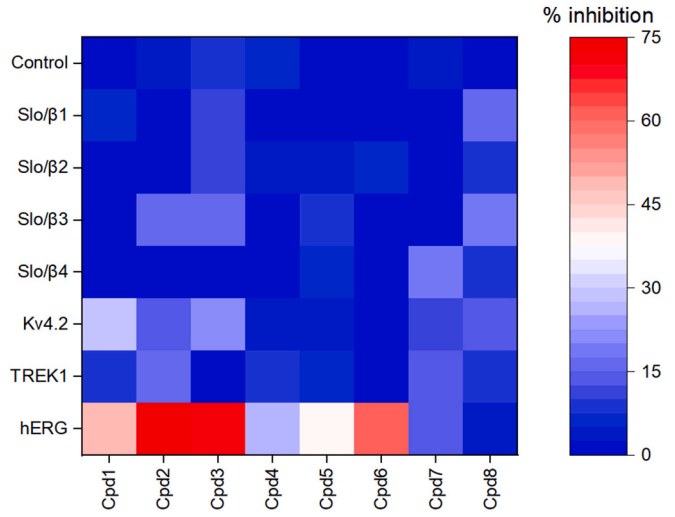

Fig. 5. Heatmap indicating mean % inhibition of control HEK293 cells or those expressing potassium channels as indicated by 10 μM of Compounds **1**–**8**. Data were obtained using thallium flux assay except for hERG, which was analysed using patch clamp electrophysiology.

3. Conclusions

This study has identified a number of novel, structurally diverse, and synthetically tractable inhibitors of the human $K_{Na}1.1$ ion channel using a combination of *in silico* large-scale virtual high-throughput screening, *in vitro* thallium flux assays and whole cell patch-clamping. This large-scale approach has led to the development of more structurally diverse and synthetically tractable compounds compared to our previous smaller screen [27]. We have shown it is possible to achieve selectivity for the $K_{Na}1.1$ channel versus other potassium channels, including hERG, which is crucial for further development of lead candidates. Due to the lack of commercially available analogues of these compounds, we are currently unable to develop the structure-activity relationship profile of these inhibitors to understand their requirements for binding. This has also limited the optimisation of the pharmacokinetic properties of these inhibitors, many of which suffer from poor aqueous solubility and low metabolic stability. The recent publication of an inhibitor-bound cryo-EM structure of human $K_{Na}1.1$ provides an enhanced scope to use the approach discussed here for the future identification and optimisation of inhibitors to treat KCNT1-related neurological disorders.

4. Materials and methods

4.1. Molecular biology and cell culture

The full-length wild-type (WT) $K_{Na}1.1$ cDNA in pcDNA6-V5/His6 vector (Invitrogen) is described previously [27]. Using this, a concatemeric construct was generated in pcDNA6 so that a second $K_{Na}1.1$ subunit containing the known Y796H GoF variant was fused to the C-terminus of the wild type $K_{Na}1.1$ with a T2A "self-cleaving" linker sequence [36]. This construct was transfected into human embryonic kidney (HEK) 293 cells (transfection and culture details provided below) and cultured in medium containing 5 μg/mL blasticidin for selection of stably transfected clones. Blasticidin-resistant colonies of HEK cells were isolated, expanded, and assessed for stable WT/Y796H $K_{Na}1.1$ currents by whole cell patch clamp recording (see electrophysiology section below).

Human embryonic kidney (HEK) 293 cells, either stably expressing or transiently transfected with the ion channel of interest, were cultured at 37 °C in air containing 5% CO_2 in Dulbecco's modified Eagle medium (DMEM with GlutaMax, Invitrogen), supplemented with 10 % foetal bovine serum, 50 U/mL penicillin, and 0.05 mg/mL streptomycin. When required, cells were transiently transfected using the TransIT-X2 reagent (Cambridge Bioscience) according to the supplier's specifications.

4.2. Compound library generation

Compound libraries from Otava (www.otavachemicals.com) and Enamine (https://enamine.net/) were downloaded in SMILES format. Three-dimensional versions of these libraries were produced using OpenEye OMEGA conformer generation software (OpenEye OMEGA Application 2022.1.1, OpenEye, Cadence Molecular Sciences, Santa Fe, NM. http://www.eyesopen.com.) [37]. Due to the large size of these libraries, only the lowest energy conformer was produced for each compound.

4.3. Virtual screening

To identify candidate compounds, high-throughput virtual screening was carried out using the ARC4 advanced research computing cluster at

the University of Leeds. Cryo-electron microscopy structures of the chicken $K_{Na}1.1$ potassium ion channel (PDB 5U76 or 5U70 [3] for the inactive and active states, respectively), were prepared using the Maestro protein preparation wizard (Schrödinger Release 2020-3, Schrödinger, LLC, New York, NY, 2024). Large libraries of commercially available compounds from Enamine and Otava, as well as an in-house library, were initially screened using the FRED docking algorithm (OpenEye FRED Application 2022.1.1, OpenEye, Cadence Molecular Sciences, Santa Fe, NM. http://www.eyesopen.com) [38] using the Chemgauss4 scoring function. Compound libraries were docked to a region of the pore domain comprising a 20 Å cube encompassing side chains from the selectivity filter and S6 transmembrane segment that line the intracellular pore vestibule (Fig. 1A). The compounds were ranked according to their Chemgauss4 docking score and the 10% top-scoring compounds subsequently rescored using Schrödinger Glide [39] in Standard Precision (SP) mode. Approximately 500 compounds were visually inspected using Maestro to identify predicted specific binding interactions with the protein (Fig. 2D) and disregard compounds with pan-assay interference structures [34]. Structurally diverse compounds with the best docking scores were purchased and tested *in vitro*.

4.4. Cell viability

Cell viability was determined using the WST-1 assay according to the manufacturer's instructions. HEK293 cells were seeded into a 96 well plate at a concentration of 5×10^4 cells per well in 100 µL of DMEM culture medium and incubated at 37 °C with 5% CO_2 overnight. Compounds of interest or positive control, consisting of 10% DMSO, were subsequently added to wells in triplicate and the cells incubated for a further 24 h, after which 10 µL of WST-1 reagent (Merck, 5015944001) was added to each well. Cells were incubated at 37 °C with 5% CO_2 for 4 h, then thoroughly shaken for 1 min before reading the absorbance of the plate 450 nm, reference wavelength 650 nm. Cell viability was calculated as a percentage of the absorbance read from untreated cells.

4.5. Thallium flux assay

All chemicals were sourced from Sigma-Aldrich (Gillingham, U.K.) unless otherwise stated. HEK293 cells were plated into a clear-bottomed, poly-D-lysine coated 96-well plate (ThermoFisher Scientific) at a density of 5×10^5 cells per well in 100 µL of DMEM culture medium and incubated at 37 °C with 5% CO_2 overnight. Cells were then washed once with chloride-free Hank's balanced salt solution (HBSS) (140 mM sodium gluconate, 5 mM potassium gluconate, 1 mM calcium gluconate, 0.9 mM magnesium sulphate heptahydrate, 0.3 mM sodium phosphate dibasic dihydrate, 0.4 mM potassium phosphate monobasic, 6 mM D-Glucose, 4 mM sodium bicarbonate, pH 7.3) and loaded with 90 µL of assay buffer consisting of 1.25 µg/mL Thallos AM dye (ION Biosciences), 0.1 % Pluronic™ F-127 (ThermoFisher Scientific) and extracellular fluorescence quenchers (5 mM tartrazine and 10 mM amaranth). 10 µL of test compound were diluted from a 10 mM DMSO stock with chloride-free HBSS and quenchers and the plate incubated at 37 °C for 1 h. For initial validation, compounds were applied at a final concentration of 10 µM, with concentration-inhibition analysis conducted on compounds selected from those that exhibited at least half of the inhibition measured with 100 µM bepridil. Following incubation, Thallos fluorescence was read every 5 s using a FlexStation 3 Microplate reader (Molecular Devices) (excitation 490 m, emission 515 nm), wherein baseline fluorescence was measured for 30 s prior to the addition of Tl_2SO_4 solution in HBSS with quenchers to a final concentration of 2.5 mM, after which fluorescence was measured for a further 150 s. The slope of the first ten measurements versus time, following thallium sulphate addition, was used as a measure of channel activity, and the slopes from the untreated wells were used as control. For concentration-inhibition analysis of selected compounds, a range of inhibitor concentrations were applied across individual well. Data were analysed in OriginPro 9.65 (OriginLab Corporation, Northampton, MA, USA) using the dose-response curve fitting function to yield IC_{50} values.

4.6. Manual patch-clamp electrophysiology

Membrane currents were measured at room temperature using patch-clamp recording in the whole-cell configuration. An EPC-10 amplifier (HEKA Electronics, Lambrecht, Germany) was used, with >65 % series resistance compensation (where appropriate), 2.9 kHz low-pass filtering, and 10 kHz digitisation as described previously [27]. HEK293 cells were seeded onto 10 mm glass cover slips a day prior to use and placed into a recording chamber connected to a gravity perfusion system. Patch pipettes with a resistance of 1.5-3.0 MΩ in experimental solution were pulled from thin-walled borosilicate glass (Harvard Apparatus Ltd, Edenbridge, Kent, UK) and polished. The extracellular recording solution for recording $K_{Na}1.1$ potassium currents contained 140 mM NaCl, 1 mM $CaCl_2$, 5 mM KCl, 29 mM Glucose, 10 mM HEPES and 1 mM $MgCl_2$, pH 7.4 with NaOH, and the pipette solution contained 100 mM K-Gluconate, 30 mM KCl, 10 mM Na-Gluconate, 29 mM Glucose, 5 mM EGTA and 10 mM HEPES, pH 7.3 with KOH. To assess the current-voltage relationship, cells were held at −80 mV and 400 ms pulses were applied at 10 mV increments between −100 and 80 mV. For inhibitor analysis, 750 ms voltage ramps were applied from −100 to +40 mV and $K_{Na}1.1$ channel activity was measured as the slope of the linear, weakly voltage-dependent component of the evoked current. Inhibition was assessed by the application of compound-containing extracellular solution via gravity perfusion, and concentration-inhibition analysis: $G/G_C = (1 + ([B]/IC_{50})^H)^{-1} + c$, where G is the conductance measured as the slope of the current evoked by the voltage ramp in the presence of the inhibitor, G_C is the control conductance in the absence of inhibitor, [B] is the concentration of the inhibitor, IC_{50} the concentration of inhibitor that yields 50% inhibition, H the slope factor, and c the residual current. Data analysis was conducted using Fitmaster (HEKA Electronics, Lambrecht, Germany), Microsoft Excel, and OriginPro 9.65.

The extracellular recording solution when recording cells expressing the hERG potassium ion channel contained 137 mM NaCl, 1.8 mM $CaCl_2$, 4 mM KCl, 10 mM Glucose, 10 mM HEPES, 1 mM $MgCl_2$, pH 7.3 with NaOH and the pipette solution contained 140 mM KCl, 10 mM EGTA, 10 mM HEPES, 2 mM $MgCl_2$, 5 mM Mg_2ATP, pH 7.2 with KOH. To assess channel inhibition, the cells were held at −80 mV and a pulse protocol of 40 mV for 4 s and then −50 mV for 4 s was applied every 20 s. Compounds were applied by gravity perfusion at the indicated concentrations and the degree of inhibition determined from the tail current (−50 mV step) amplitude.

Funding sources

This work was supported by Action Medical Research (grant number GN2865). BAC was supported a BBSRC-CASE PhD studentship (BB/M011151/1) in conjunction with Autifony Therapeutics Ltd. AJF was supported by a Wellcome Trust PhD studentship.

CRediT authorship contribution statement

Emily A. Caseley: Formal analysis, Investigation, Methodology, Visualization, Writing – original draft. **Katie J. Simmons:** Conceptualization, Funding acquisition, Methodology, Supervision, Writing – original draft. **Bethan A. Cole:** Methodology, Resources. **Alex J. Flynn:** Investigation, Methodology. **Stephen P. Muench:** Conceptualization, Funding acquisition, Writing – original draft. **Jonathan D. Lippiat:** Conceptualization, Funding acquisition, Project administration, Resources, Supervision, Visualization, Writing – original draft.

Declaration of competing interest

The authors declare that they have no known competing financial interests or personal relationships that could have appeared to influence the work reported in this paper.

Acknowledgements

This work was undertaken on ARC4, part of the High-Performance Computing facilities at the University of Leeds, UK.

Appendix A. Supplementary data

Supplementary data to this article can be found online at https://doi.org/10.1016/j.ejmech.2026.118906.

Data availability

Data will be made available on request.

References

[1] L. Salkoff, et al., High-conductance potassium channels of the SLO family, Nat. Rev. Neurosci. 7 (12) (2006) 921–931.
[2] A. Yuan, et al., The sodium-activated potassium channel is encoded by a member of the Slo gene family, Neuron 37 (5) (2003) 765–773.
[3] R.K. Hite, R. MacKinnon, Structural titration of Slo2.2, a Na+-Dependent K+ channel, Cell 168 (3) (2017) 390–399.e11.
[4] J. Zhang, et al., Structural basis of human Slo2.2 channel gating and modulation, Cell Rep. 42 (8) (2023).
[5] H. Chen, et al., The N-terminal domain of Slack determines the formation and trafficking of Slick/Slack heteromeric sodium-activated potassium channels, J. Neurosci. 29 (17) (2009) 5654–5665.
[6] X. Mao, et al., The Epilepsy of Infancy With Migrating Focal Seizures: identification of de novo Mutations of the KCNT2 Gene That Exert Inhibitory Effects on the Corresponding Heteromeric K(Na)1.1/K(Na)1.2 Potassium Channel, Front. Cell. Neurosci. 14 (2020) 1.
[7] S. Franceschetti, et al., Na+-activated K+ current contributes to postexcitatory hyperpolarization in neocortical intrinsically bursting neurons, J. Neurophysiol. 89 (4) (2003) 2101–2111.
[8] X. Liu, L. Stan Leung, Sodium-activated potassium conductance participates in the depolarizing afterpotential following a single action potential in rat hippocampal CA1 pyramidal cells, Brain Res. 1023 (2) (2004) 185–192.
[9] B. Yang, R. Desai, L. Kaczmarek, Slack and slick KNa channels regulate the accuracy of timing of auditory neurons, J. Neurosci. : the official journal of the Society for Neuroscience 27 (2007) 2617–2627.
[10] K.M. Evely, et al., Slack K(Na) channels Influence Dorsal horn synapses and nociceptive behavior, Mol. Pain 13 (2017) 1744806917714342.
[11] J.H. Lee, et al., The local translation of K(Na) in dendritic projections of auditory neurons and the roles of K(Na) in the transition from hidden to overt hearing loss, Aging (Albany NY) 11 (23) (2019) 11541–11564.
[12] P. Li, et al., Sodium-activated potassium channels moderate excitability in vascular smooth muscle, J. Physiol. 597 (20) (2019) 5093–5108.
[13] B.A. Cole, et al., *Targeting $K_{Na}1.1$ channels in KCNT1-associated epilepsy*, Trends Pharmacol. Sci. 42 (8) (2021) 700–713.
[14] G. Barcia, et al., De novo gain-of-function KCNT1 channel mutations cause malignant migrating partial seizures of infancy, Nat. Genet. 44 (11) (2012) 1255–1259.
[15] S.E. Heron, et al., Missense mutations in the sodium-gated potassium channel gene KCNT1 cause severe autosomal dominant nocturnal frontal lobe epilepsy, Nat. Genet. 44 (11) (2012) 1188–1190.
[16] H.C. Martin, et al., Clinical whole-genome sequencing in severe early-onset epilepsy reveals new genes and improves molecular diagnosis, Hum. Mol. Genet. 23 (12) (2014) 3200–3211.
[17] C. Ohba, et al., De novo KCNT1 mutations in early-onset epileptic encephalopathy, Epilepsia 56 (9) (2015) e121–e128.
[18] Y. Jia, et al., Quinidine therapy for lennox-gastaut syndrome with KCNT1 mutation. A case report and literature review, Front. Neurol. 10 (2019), 2019.
[19] C.X. Lim, et al., KCNT1 mutations in seizure disorders: the phenotypic spectrum and functional effects, J. Med. Genet. 53 (4) (2016) 217–225.
[20] C.M. Bonardi, et al., KCNT1-related epilepsies and epileptic encephalopathies: phenotypic and mutational spectrum, Brain 144 (12) (2021) 3635–3650.
[21] B. Yang, et al., Pharmacological activation and inhibition of Slack (Slo2.2) channels, Neuropharmacology 51 (4) (2006) 896–906.
[22] M.P. Fitzgerald, et al., Treatment responsiveness in KCNT1-Related epilepsy, Neurotherapeutics 16 (3) (2019) 848–857.
[23] D. Xu, et al., Precision therapy with quinidine of KCNT1-related epileptic disorders: a systematic review, Br. J. Clin. Pharmacol. 88 (12) (2022) 5096–5112.
[24] R. Liu, et al., New use for an old drug: quinidine in KCNT1-related epilepsy therapy, Neurol. Sci. 44 (4) (2023) 1201–1206.
[25] N.J. White, Cardiotoxicity of antimalarial drugs, Lancet Infect. Dis. 7 (8) (2007) 549–558.
[26] I. Mosca, et al., Case report: marked electroclinical improvement by fluoxetine treatment in a patient with KCNT1-related drug-resistant focal epilepsy, Front. Cell. Neurosci. 18 (2024) 1367838.
[27] B.A. Cole, et al., Structure-Based identification and characterization of inhibitors of the epilepsy-associated K(Na)1.1 (KCNT1) potassium channel, iScience 23 (5) (2020) 101100.
[28] B.D. Spitznagel, et al., VU0606170, a selective slack channels inhibitor, decreases calcium oscillations in cultured cortical neurons, ACS Chem. Neurosci. 11 (21) (2020) 3658–3671.
[29] A.M. Griffin, et al., Discovery of the first orally available, selective K(Na)1.1 inhibitor: *in vitro* and *in vivo* activity of an oxadiazole series, ACS Med. Chem. Lett. 12 (4) (2021) 593–602.
[30] A.a.M. Qunies, et al., Design, synthesis, and biological evaluation of a novel series of 1,2,4-oxadiazole inhibitors of SLACK potassium channels: identification of in vitro tool VU0935685, Bioorg. Med. Chem. 95 (2023) 117487.
[31] N. Iraci, et al., In silico assisted identification, synthesis, and in vitro pharmacological characterization of potent and selective blockers of the epilepsy-associated KCNT1 channel, J. Med. Chem. 67 (11) (2024) 9124–9149.
[32] R.K. Hite, et al., Cryo-electron microscopy structure of the Slo2.2 Na+-activated K + channel, Nature 527 (7577) (2015) 198–203.
[33] M. Batool, B. Ahmad, S. Choi, A structure-based drug Discovery paradigm, Int. J. Mol. Sci. 20 (11) (2019) 2783.
[34] J.B. Baell, G.A. Holloway, New substructure filters for removal of Pan Assay Interference compounds (PAINS) from screening libraries and for their exclusion in bioassays, J. Med. Chem. 53 (7) (2010) 2719–2740.
[35] J. Zhang, et al., Endogenous ion channels expressed in human embryonic kidney (HEK-293) cells 474 (7) (2022) 665–680.
[36] M.G. Ricos, et al., Identification of new KCNT1-epilepsy drugs by in silico, cell and Drosophila modelling, bioRxiv (2025), 2025.05.22.655336.
[37] P.C. Hawkins, et al., Conformer generation with OMEGA: algorithm and validation using high quality structures from the Protein Databank and Cambridge Structural Database, J. Chem. Inf. Model. 50 (4) (2010) 572–584.
[38] M. McGann, FRED pose prediction and virtual screening accuracy, J. Chem. Inf. Model. 51 (3) (2011) 578–596.
[39] T.A. Halgren, et al., Glide: a new approach for rapid, accurate docking and scoring. 2. Enrichment factors in database screening, J. Med. Chem. 47 (7) (2004) 1750–1759.